
THE MIXED DEEP ENERGY METHOD FOR RESOLVING CONCENTRATION FEATURES IN FINITE STRAIN HYPERELASTICITY

A PREPRINT

Jan Niklas Fuhg

Sibley School of Mechanical and Aerospace Engineering
Cornell University, New York, USA
jf853@cornell.edu

Nikolaos Bouklas

Sibley School of Mechanical and Aerospace Engineering
Cornell University, New York, USA
nb589@cornell.edu

January 7, 2022

ABSTRACT

The introduction of Physics-informed Neural Networks (PINNs) has led to an increased interest in deep neural networks as universal approximators of PDEs in the solid mechanics community. Recently, the Deep Energy Method (DEM) has been proposed. DEM is based on energy minimization principles, contrary to PINN which is based on the residual of the PDEs. A significant advantage of DEM, is that it requires the approximation of lower order derivatives compared to formulations that are based on strong form residuals. However both DEM and classical PINN formulations struggle to resolve fine features of the stress and displacement fields, for example concentration features in solid mechanics applications. We propose an extension to the Deep Energy Method (DEM) to resolve these features for finite strain hyperelasticity. The developed framework termed mixed Deep Energy Method (mDEM) introduces stress measures as an additional output of the NN to the recently introduced pure displacement formulation. Using this approach, Neumann boundary conditions are approximated more accurately and the accuracy around spatial features which are typically responsible for high concentrations is increased. In order to make the proposed approach more versatile, we introduce a numerical integration scheme based on Delaunay integration, which enables the mDEM framework to be used for random training point position sets commonly needed for computational domains with stress concentrations, i.e. domains with holes, notches, etc. We highlight the advantages of the proposed approach while showing the shortcomings of classical PINN and DEM formulations. The method is offering comparable results to Finite-Element Method (FEM) on the forward calculation of challenging computational experiments involving domains with fine geometric features and concentrated loads, but additionally offers unique capabilities for the solution of inverse problems and parameter estimation in the context of hyperelasticity.

Keywords Physics-informed neural networks · Deep energy method · Mixed deep energy method · Solid mechanics · Hyperelasticity · Finite Strain

1 Introduction

Solid mechanics studies the motion and deformation of solid materials when subjected to external forces. In the last years we have seen a rapid growth in the utilization of machine learning and data-driven techniques in computational

solid mechanics. For example, Kirchdoerfer and Ortiz (2016) defined a computational data-driven approach that enforces constraints and conservation laws directly on experimental data. This data-driven approach has been extended to a wide range of directions such as inelastic problems (Eggersmann et al., 2019) and also extended to a non-local setting (González et al., 2019). Machine learning has also been used to establish data-driven elastic and inelastic constitutive laws (Fuhg et al., 2021; Huang et al., 2020; Ibañez et al., 2017). These ideas make use of existing infrastructures such as existing Finite-Element Method (FEM) solvers to solve the accompanying partial differential equations (PDEs). Additionally, machine learning techniques have been employed for the development of intrusive and non-intrusive Reduced Order Modeling (ROM) schemes for the accelerated solutions of PDEs (Hernandez et al., 2021; Kadeethum et al., 2021) following the offline-online paradigm, in which synthetic training data is often constructed from FEM solvers.

As an alternative approach, Neural Networks (NN) have recently gained a lot of attention in the solid mechanics community, and more broadly in the physic-based modeling community, for finding solutions of boundary value problems from scratch, due to their abilities as universal approximators (Hornik et al., 1989). While the idea is not new and has already been proposed over 20 years ago (Lagaris et al., 1998), it has seen remarkable success recently due to advances in GPU hardware and neural network technologies (e.g. deep learning libraries, stochastic gradient descent algorithms, etc). In this context Physics-informed Neural Networks (PINNs), first introduced in Raissi et al. (2019), have emerged as a deep learning algorithm for solving PDEs, based on automatic differentiation. The method has several advantages compared to classical numerical techniques with the major ones being that the algorithm is meshfree and is significantly easier to implement than traditional methods such as FEM while at the same time allows for the incorporation of constraints due to experimental observations and solution of inverse problems for parameter estimation. As PINN is an optimization-based solution technique, it also has the potential to be utilized in highly nonlinear problems where traditional solution techniques are not sufficient or necessarily robust. PINN has been extended into different directions such as variational problems (VPINN) (Kharazmi et al., 2021) or a subdomain-version (XPINN) which defines local neural networks in order to allow parallelization of the computation and also to resolve the solution in heterogeneous domains (Jagtap and Karniadakis, 2020).

From these ideas different approaches have been developed to utilize PINNs for applications in solid mechanics. Haghighat et al. (2020) trained PINN for small strain elasticity and elastoplasticity problems, Kadeethum et al. (2020) used the approach to solve the coupled Biot's equations, and Rao et al. (2020) explored a mixed formulation for regular physics-informed neural networks with applications to small strain elastodynamics problems. Abueidda et al. (2020) utilized the residual formulation of PINNs to study linear elasticity, hyperelasticity, and plasticity. Recently, the Deep Energy Method (DEM) was introduced, which defines the loss function not based on residual equations but based on energy minimization principles (Nguyen-Thanh et al., 2020; Samaniego et al., 2020; Weinan and Yu, 2018). Compared to classical PINN, this method has advantages because it only requires first order differentiation through the neural network. On the other hand it relies on accurate numerical integration techniques. With this technique Nguyen-Thanh et al. (2020) solve two and three dimensional finite-strain hyperelastic problems. However as will be shown in this work, both the PINN and DEM struggle to resolve displacement and stress concentrations. In this context we propose the mixed Deep Energy Method (mDEM) which, by requiring both displacements and stress outputs from the NN architecture, is able to resolve concentration features on comparable levels to FEM. Hence, the presented method aims to improve the forward capabilities of the physics-informed machine learning paradigm for solid mechanics applications as a first step towards efficient and accurate inverse problem calculations. Furthermore we provide some extension to the initial DEM formulation by offering a more reliable integration scheme based on Delaunay triangulation.

In section 2 the general finite-strain solid mechanics framework for hyperelasticity is introduced, and specialized to a Neo-Hookean type strain energy. A short introduction to neural networks, PINNs and DEMs specialized for 2D hyperelasticity is provided in Section 3. The newly proposed mixed Deep Energy Method formulation as well as an accompanying integration scheme based on Delaunay triangulation are introduced in Section 4. In Section 5 we test the approach on various computational experiments comparing against existing PINN- and DEM-based implementations. The paper is concluded in Section 6.

2 Finite-strain hyperelasticity

Let a bounded domain be occupied by an elastic body $\mathcal{B} \subset \mathbb{R}^3$. The body's boundary Γ consists of two non-overlapping regions Γ_t and Γ_u such that $\Gamma = \Gamma_t \cup \Gamma_u$ (Fig. 1). Let the referential and current position vectors of the body be denoted by \mathbf{X} and \mathbf{x} respectively. The time-dependent motion between the two positions is then given by

$$\mathbf{x} = \boldsymbol{\varphi}(\mathbf{X}, t) = \mathbf{X} + \mathbf{u}(\mathbf{X}, t) \quad (1)$$

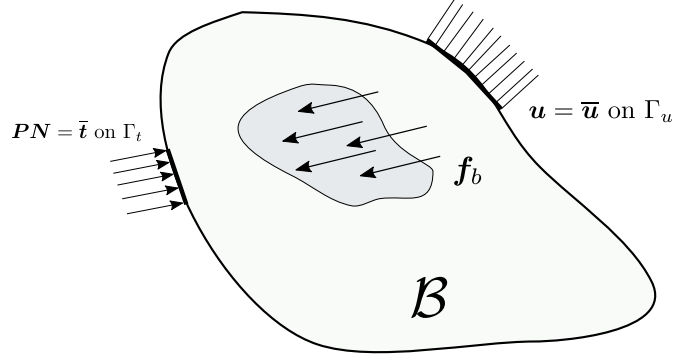


Figure 1: Solid domain with boundary conditions

with $\varphi(\mathbf{X}, t)$ denoting the motion of the body and \mathbf{u} the time-dependent displacement field. The gradient of the motion with respect to the initial position yield the deformation gradient

$$\mathbf{F} = \text{Grad}\varphi(\mathbf{X}). \quad (2)$$

The governing equation for quasi-static problems in solid continua is the equilibrium equation, which in strong form reads

$$\text{Div}\mathbf{P} + \mathbf{f}_b = \mathbf{0}, \quad \text{in } \mathcal{B} \quad (3)$$

with

$$\begin{aligned} \mathbf{u} &= \tilde{\mathbf{u}} & \text{on } \Gamma_u, \\ \mathbf{P} \cdot \mathbf{N} &= \tilde{\mathbf{t}} & \text{on } \Gamma_t, \end{aligned} \quad (4)$$

where \mathbf{P} and \mathbf{f}_b denote the first Piola-Kirchhoff stress tensor and the body force vector respectively. The body is in general subjected to two types of boundary conditions with the outward normal \mathbf{N} , the prescribed displacement $\tilde{\mathbf{u}}$ on Γ_t and the prescribed surface traction $\tilde{\mathbf{t}}$ on Γ_u as denoted in eq. 4.

In the hyperelastic framework, the existence of the strain energy function Ψ is postulated, which enables the computation of the first Piola-Kirchhoff stress tensor by

$$\mathbf{P} = \frac{\partial \Psi}{\partial \mathbf{F}}. \quad (5)$$

In this paper we define a Neo-Hookean type strain energy which allows for compressibility as

$$\Psi = \frac{1}{4}\lambda(\log J^2 - 1 - 2\log J) + \frac{1}{2}\mu(\text{tr}(\mathbf{C}) - 2 - 2\log J), \quad (6)$$

where λ and μ are the Lamé constants and J and \mathbf{C} are given by $J = \det \mathbf{F}$ and $\mathbf{C} = \mathbf{F}^T \mathbf{F}$. Considering only conservative loads and neglecting inertial contributions, the potential energy of the body is defined by

$$\Pi(\varphi) = \int_{\mathcal{B}} \Psi dV - \int_{\mathcal{B}} \mathbf{f}_b \cdot \varphi dV - \int_{\Gamma_t} \tilde{\mathbf{t}} \cdot \varphi dA. \quad (7)$$

The energy functional from eq. 7 can be minimized with regards to φ which yields the deformation that fulfills static equilibrium.

3 Deep neural networks, Physics-informed Neural Networks and the Deep Energy Method

In this section we provide a brief overview of the neural networks formulation, Physics-informed Neural Networks and the Deep Energy Method. Neural networks are in general composed of one input, one output and $n_D - 1$ hidden layers. Let the weights and biases of the k^{th} layer be denoted by \mathbf{W}^k and \mathbf{b}^k . Consider that the k^{th} hidden layer transfers some output \mathbf{x}^k to the $(k + 1)^{\text{th}}$ layers which applies an affine transformation

$$\mathcal{L}(\mathbf{x}^k) = \mathbf{W}^{k+1} \mathbf{x}^k + \mathbf{b}^{k+1}. \quad (8)$$

and some activation function σ to it. We consider the activation function of the last layer to be identity. Since, equation (8) is applied in every layer of the network an input \mathbf{x} yields a network output of the form

$$\hat{\mathbf{y}}(\mathbf{x}) = (\mathcal{L}_k \circ \sigma \circ \mathcal{L}_{k-1} \circ \cdots \circ \sigma \circ \mathcal{L}_1)(\mathbf{x}) \quad (9)$$

where \circ is a composition operator. The goal of neural networks is to find the optimal value set of trainable parameters $\Theta = \{\mathbf{W}^k, \mathbf{b}^k\}_{k=1}^{n_D}$ such that the networks provides the best fit for the input-output mapping. This is achieved by following an optimization procedure defined over some loss function $J(\Theta)$

$$\Theta^* = \arg \min_{\Theta} J(\Theta). \quad (10)$$

This problem is typically solved in an iterative manner by employing a stochastic gradient-descent approach. A review on neural network optimization methods is provided in Bottou et al. (2018). For more information on neural networks we refer to Goodfellow et al. (2016).

PINNs define a global shape function for the field(s) of interest over the computational domain and then require the stresses derived with automatic differentiation to fulfill a residual based on the strong form, including the equilibrium equation (3) as well as the corresponding boundary conditions (4). The computational domain is spanned by a set of collocation points. Here we will specialize the overview of PINN in the context of hyperelasticity. In this case the unknown field that will be approximated through PINN is the displacement field. In absence of body forces, the residual is of the form

$$\mathcal{R} = \text{Div} \mathbf{P} = \mathbf{0}. \quad (11)$$

The collocation points hereby act as inputs to the neural network which yield the outputs $z(\mathbf{X}, \Theta)$. The outputs $z(\mathbf{X}, \Theta)$ can either be subjected to

$$\hat{\mathbf{u}}(\mathbf{X}, \Theta) = \mathbf{A}(\mathbf{X}) + \mathbf{B}(\mathbf{X}) \circ z(\mathbf{X}, \Theta) \quad (12)$$

where \mathbf{A} and \mathbf{B} are a-priori chosen in a way such that the displacement prediction $\hat{\mathbf{u}}$ fulfills the displacement boundary conditions acting on the body. Here, \mathbf{A} and \mathbf{B} can either chosen analytically or can be neural networks themselves. For a detailed discussion refer to Rao et al. (2020). Alternately, we can choose

$$\hat{\mathbf{u}}(\mathbf{X}, \Theta) = z(\mathbf{X}, \Theta) \quad (13)$$

where the boundary conditions need to be trained. From the displacements the deformation gradient can be obtained by

$$\hat{\mathbf{F}}(\mathbf{X}, \Theta) = \mathbf{I} + \text{Grad} \hat{\mathbf{u}}(\mathbf{X}, \Theta). \quad (14)$$

Consequently, the stresses $\mathbf{P}(\hat{\mathbf{F}}(\mathbf{X}, \Theta))$ can be computed following their definitions eq. 5.

Consider a set of domain training points $\{\mathbf{X}_{\mathcal{R}}^i\}_{i=1}^{N_{\mathcal{R}}}$, displacement boundary training points $\{\mathbf{X}_u^i\}_{i=1}^{N_u}$ and traction boundary training points $\{\mathbf{X}_t^i\}_{i=1}^{N_t}$ where $N_{\mathcal{R}}$, N_u and N_t denote the number of points, respectively. The PINN loss function is then defined as

$$\Theta^* = \arg \min_{\Theta} \quad W_{\mathcal{R}} \text{MSE}_{\mathcal{R}} \left(\{\mathbf{X}_{\mathcal{R}}^i\}_{i=1}^{N_{\mathcal{R}}}, \Theta \right) + W_t \text{MSE}_t \left(\{\mathbf{X}_t^i\}_{i=1}^{N_t}, \Theta \right) + \underbrace{W_u \text{MSE}_u \left(\{\mathbf{X}_u^i\}_{i=1}^{N_u}, \Theta \right)}_{\text{If not a-priori fulfilled}} \quad (15)$$

with some weight values $W_{\mathcal{R}}$, W_t and W_u and specializing to a 2D case

$$\begin{aligned} \text{MSE}_{\mathcal{R}} \left(\{\mathbf{X}_{\mathcal{R}}^i\}_{i=1}^{N_{\mathcal{R}}}, \Theta \right) &= \frac{1}{N_{\mathcal{R}}} \sum_{i=1}^{N_{\mathcal{R}}} \left| \frac{\partial}{\partial X_1} P_{11}(\hat{\mathbf{F}}(\mathbf{X}_{\mathcal{R}}^i, \Theta)) + \frac{\partial}{\partial X_2} P_{12}(\hat{\mathbf{F}}(\mathbf{X}_{\mathcal{R}}^i, \Theta)) \right|^2 \\ &\quad + \frac{1}{N_{\mathcal{R}}} \sum_{i=1}^{N_{\mathcal{R}}} \left| \frac{\partial}{\partial X_1} P_{21}(\hat{\mathbf{F}}(\mathbf{X}_{\mathcal{R}}^i, \Theta)) + \frac{\partial}{\partial X_2} P_{22}(\hat{\mathbf{F}}(\mathbf{X}_{\mathcal{R}}^i, \Theta)) \right|^2, \\ \text{MSE}_t \left(\{\mathbf{X}_t^i\}_{i=1}^{N_t}, \Theta \right) &= \frac{1}{N_t} \sum_{i=1}^{N_t} \left| \mathbf{P}(\hat{\mathbf{F}}(\mathbf{X}_t^i, \Theta)) \mathbf{N}_i - \bar{\mathbf{t}}(\mathbf{X}_t^i) \right|^2, \\ \text{MSE}_u \left(\{\mathbf{X}_u^i\}_{i=1}^{N_u}, \Theta \right) &= \frac{1}{N_u} \sum_{i=1}^{N_u} \left| \hat{\mathbf{u}}(\mathbf{X}_u^i, \Theta) - \mathbf{u}(\mathbf{X}_u^i) \right|^2. \end{aligned} \quad (16)$$

The PINN concept is summarized in Figure 2. Maintaining some of the architecture of PINNs, Nguyen-Thanh et al. (2020) proposed an alternative approach. The neural network formulation is still used to solve quasi-static equilibrium problems by utilizing the network as a global shape function for the displacement over the body. However instead of defining the residual of the governing PDE as the loss function, the authors define the loss as the potential energy of the solid body, as defined in equation 7. By following that, the minimization of the loss function over some collocation points that span the computational domain and its boundary, through stationarity of the potential energy in

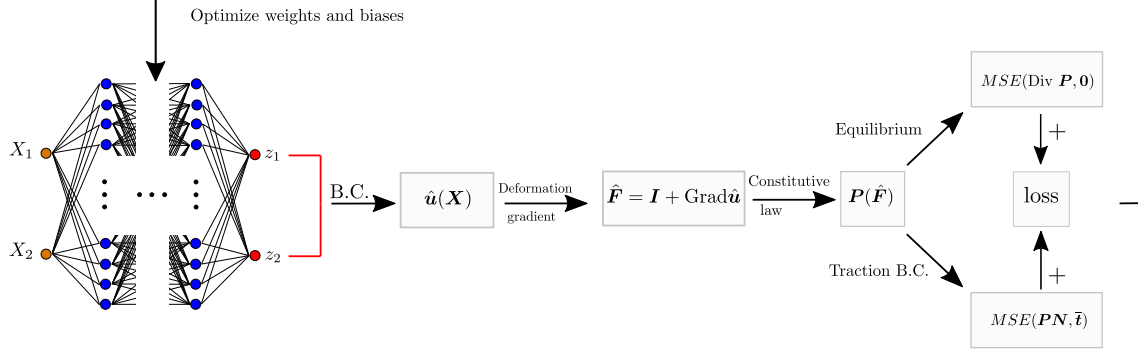


Figure 2: PINN overview

nonlinear problems, leads to an approximate solution. The advantage of this approach is that only first order automatic differentiation is needed for the solution procedure, instead of second order as required in PINN. This, can potentially lead to quicker convergence and higher accuracy. As a downside the method requires an effective integration procedure over the domain spanned by the collocation points. In essence DEM uses the same concept as PINNs for the input and the output to the neural network, i.e. collocation point positions as input and the output is defined by either eq. 12 or 13. In addition to the deformation gradient (eq. 14), DEM requires a formulation for the motion which is given by

$$\hat{\varphi}(\mathbf{X}, \Theta) = \mathbf{X} + \hat{\mathbf{u}}(\mathbf{X}, \Theta). \quad (17)$$

Consider a set of domain training points $\{\mathbf{X}_{\Pi}^i\}_{i=1}^{N_{\Pi}}$ and boundary training points $\{\mathbf{X}_u^i\}_{i=1}^{N_u}$ where N_{Π} and N_u denote the number of points, respectively. Hence, the loss function can be written as

$$\Theta^* = \arg \min_{\Theta} \quad \Pi(\hat{\varphi}(\{\mathbf{X}_{\Pi}^i\}_{i=1}^{N_{\Pi}}, \Theta)) + \underbrace{W_u \text{MSE}_u(\{\mathbf{X}_u^i\}_{i=1}^{N_u}, \Theta)}_{\text{If not a-priori fulfilled}} \quad (18)$$

with a weight value W_u and where

$$\begin{aligned} \Pi(\hat{\varphi}(\{\mathbf{X}_{\Pi}^i\}_{i=1}^{N_{\Pi}}, \Theta)) &= \int_B \Psi(\hat{\mathbf{F}}(\{\mathbf{X}_{\Pi}^i\}_{i=1}^{N_{\Pi}}, \Theta)) dV - \int_B \mathbf{f}_b \cdot \hat{\varphi}(\{\mathbf{X}_{\Pi}^i\}_{i=1}^{N_{\Pi}}, \Theta) dV - \int_{\Gamma_t} \bar{\mathbf{t}} \cdot \hat{\varphi}(\{\mathbf{X}_{\Pi}^i\}_{i=1}^{N_{\Pi}}, \Theta) dA \\ \text{MSE}_u(\{\mathbf{X}_u^i\}_{i=1}^{N_u}, \Theta) &= \frac{1}{N_u} \sum_{i=1}^{N_u} |\hat{\mathbf{u}}(\mathbf{X}_u^i, \Theta) - \mathbf{u}(\mathbf{X}_u^i)|^2. \end{aligned} \quad (19)$$

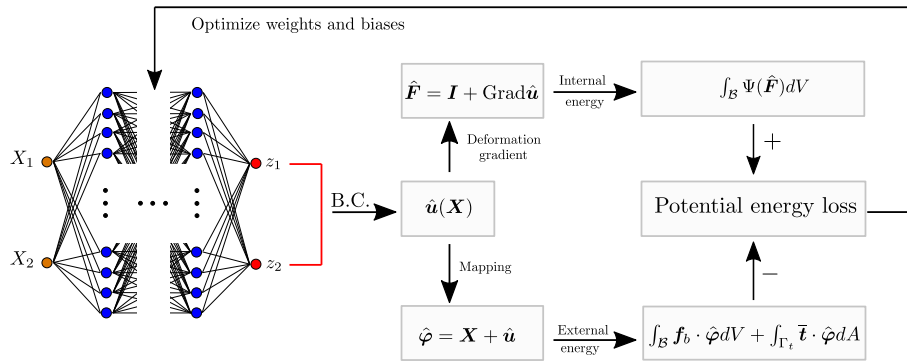


Figure 3: DEM overview

The process is summarized in Figure 3.

4 Mixed Deep Energy Method (MDEM)

For solid mechanics and multiphysics applications, problematic for the DEM and PINN formulations is that they average out stress and displacement concentrations as will be shown in Section 5. In order to circumvent these issues

we propose the Mixed Deep Energy Method (mDEM) which introduces stresses as additional collocation point outputs, which in turn have to fulfill the traction boundary conditions. Furthermore to reduce the computation time, training a different neural network for each individual output, as e.g. proposed in Haghighat et al. (2020), has been explicitly avoided in this work. Hence, in a 2D setting, in addition to the two outputs z from DEM we also obtain four more outputs Z corresponding to the first Piola-Kirchhoff stress components. Equivalently these outputs can individually be trained to directly fulfill the corresponding Dirichlet and Neumann boundary conditions respectively, or can be subjected to

$$\begin{aligned}\hat{u}(\mathbf{X}, \Theta) &= \mathbf{A}(\mathbf{X}) + \mathbf{B}(\mathbf{X}) \circ \mathbf{z}(\mathbf{X}, \Theta) \\ \hat{P}(\mathbf{X}, \Theta) &= \mathbf{C}(\mathbf{X}) + \mathbf{D}(\mathbf{X}) \circ \mathbf{Z}(\mathbf{X}, \Theta)\end{aligned}\quad (20)$$

such that these conditions are fulfilled a-priori. In order to connect the displacements and stresses, mDEM requires training of the constitutive behavior by enforcing

$$\hat{P}(\mathbf{X}, \Theta) = P(\hat{F}(\mathbf{X}, \Theta)) \quad (21)$$

where the latter term is derived from the displacement output and the hyperelastic constitutive behavior of equation (5).

Therefore we consider a set of domain training points $\{\mathbf{X}_{\Pi}^i\}_{i=1}^{N_{\Pi}}$, displacement boundary condition points $\{\mathbf{X}_u^i\}_{i=1}^{N_u}$, and traction boundary condition points $\{\mathbf{X}_t^i\}_{i=1}^{N_t}$, where N_{Π} , N_u and N_t denote the number of points. The loss function can be written as

$$\begin{aligned}\Theta^* = \arg \min_{\Theta} \quad & \Pi(\hat{\varphi}(\{\mathbf{X}_{\Pi}^i\}_{i=1}^{N_{\Pi}}, \Theta)) + W_P \text{MSE}_P(\{\mathbf{X}_{\Pi}^i\}_{i=1}^{N_{\Pi}}, \Theta) \\ & + \underbrace{W_u \text{MSE}_u(\{\mathbf{X}_u^i\}_{i=1}^{N_u}, \Theta)}_{\text{If not a-priori fulfilled}} + \underbrace{W_t \text{MSE}_t(\{\mathbf{X}_t^i\}_{i=1}^{N_t}, \Theta)}_{\text{If not a-priori fulfilled}}\end{aligned}\quad (22)$$

with weight values W_u, W_t, W_P and where

$$\begin{aligned}\Pi(\hat{\varphi}(\{\mathbf{X}_{\Pi}^i\}_{i=1}^{N_{\Pi}}, \Theta)) &= \int_B \Psi(\hat{F}(\{\mathbf{X}_{\Pi}^i\}_{i=1}^{N_{\Pi}}, \Theta)) dV - \int_B \mathbf{f}_b \cdot \hat{\varphi}(\{\mathbf{X}_{\Pi}^i\}_{i=1}^{N_{\Pi}}, \Theta) dV - \int_{\Gamma_t} \bar{\mathbf{t}} \cdot \hat{\varphi}(\{\mathbf{X}_{\Pi}^i\}_{i=1}^{N_{\Pi}}, \Theta) dA, \\ \text{MSE}_P(\{\mathbf{X}_{\Pi}^i\}_{i=1}^{N_{\Pi}}, \Theta) &= \frac{1}{N_{\Pi}} \sum_{i=1}^{N_{\Pi}} \left| \hat{P}(\mathbf{X}_{\Pi}^i, \Theta) - P(\hat{F}(\mathbf{X}_{\Pi}^i, \Theta)) \right|^2, \\ \text{MSE}_u(\{\mathbf{X}_u^i\}_{i=1}^{N_u}, \Theta) &= \frac{1}{N_u} \sum_{i=1}^{N_u} \left| \hat{u}(\mathbf{X}_u^i, \Theta) - \mathbf{u}(\mathbf{X}_u^i) \right|^2, \\ \text{MSE}_t(\{\mathbf{X}_t^i\}_{i=1}^{N_t}, \Theta) &= \frac{1}{N_t} \sum_{i=1}^{N_t} \left| \hat{P}(\mathbf{X}_t^i, \Theta) N_i - \bar{\mathbf{t}}(\mathbf{X}_t^i) \right|^2.\end{aligned}\quad (23)$$

The process is visualized in Figure 4.

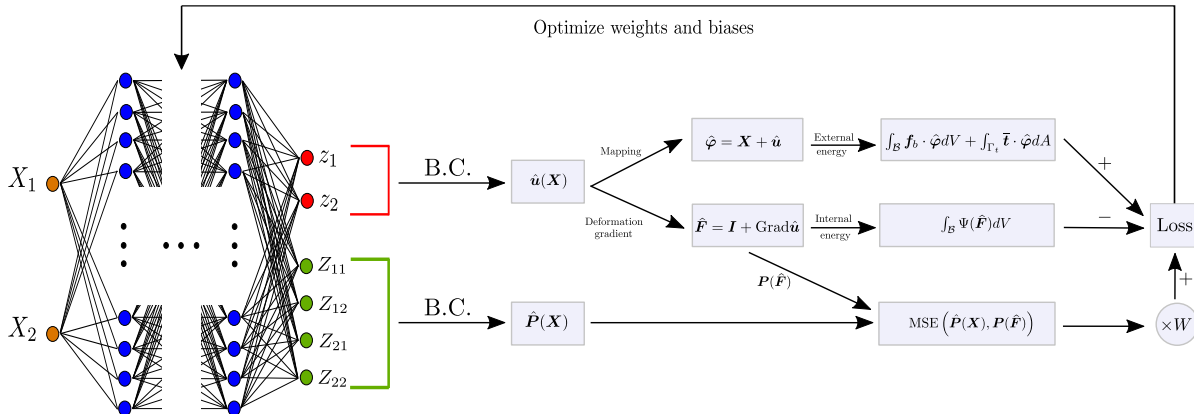


Figure 4: DEM overview



Figure 5: Constraint Voronoi tessellation for integration of defected area.

4.1 Delaunay integration

In the DEM paper (Nguyen-Thanh et al., 2020), the authors explore different numerical integration techniques for the evaluation of the integral including Trapezoidal and Simpson's rule as well as a Monte Carlo integration version. Even though the presented techniques prove to be sufficient for the investigated numerical examples, they are difficult to employ when the sample points need to represent solid continua with fine geometric features, which commonly lead to stress concentrations. Hence, in this paper we employ a form of Delaunay-integration to resolve this issue. The computational domain is tessellated based on its respective sample positions resulting in n_e triangles or tetrahedra. Given a triangle j in two dimensions, with the three points denoted by $P_i = x_i, y_i$ and a corresponding function value f_i with $i = 1, 2, 3$ for the field of interest given at each point. Then define J_j as the area of the triangle and let

$$\overline{f_{\Delta_j}} = \frac{f_1 + f_2 + f_3}{3} \quad (24)$$

denote the mean function value of an element. Following eq. 7, the potential energy of the domain is then approximated by

$$\begin{aligned} \Pi(\varphi) &= \int_B \Psi dV - \int_B \mathbf{f}_b \cdot \boldsymbol{\varphi} dV - \int_{\Gamma_t} \tilde{\mathbf{t}} \cdot \boldsymbol{\varphi} dA \\ &= \sum_{i=1}^{n_e} \int_{\Delta_i} \Psi_{\Delta_i} d\Delta_i - \sum_{i=1}^{n_e} \int_{\Delta_i} [\mathbf{f}_b \cdot \boldsymbol{\varphi}]_{\Delta_i} d\Delta_i - \int_{\Gamma_t} \tilde{\mathbf{t}} \cdot \boldsymbol{\varphi} dA \\ &= \sum_{i=1}^{n_e} J_i \overline{\Psi_{\Delta_i}} - \sum_{i=1}^{n_e} J_i \overline{[\mathbf{f}_b \cdot \boldsymbol{\varphi}]_{\Delta_i}} - \sum_{i=1}^{N_b} w_i [\tilde{\mathbf{t}}_i \cdot \boldsymbol{\varphi}_i] \end{aligned} \quad (25)$$

where w_i represents some weights to a common numerical integration technique such as Simpson's rule. An example of a constraint Voronoi mesh for a plate with a "C"-shaped hole (red zone) is displayed in Figure 5.

5 Numerical examples

In this section we compare the solutions of mDEM to DEM and PINN as well as to a Finite-Element Method (FEM) solution which will be taken as ground truth. The FEM results were obtained using the Fenics framework (Alnæs et al., 2015). The deep learning formulations were implemented¹ in Pytorch (Paszke et al., 2019) and the network parameters were optimized using the Adam optimizer (Kingma and Ba, 2014) and the limited Broyden–Fletcher–Goldfarb–Shanno (LFBGS) algorithm consecutively. In the following, we use analytical formulations to fulfill the displacement boundary conditions of the applications a-priori, while the traction boundaries are learned from data. All neural networks are composed of 6 hidden layers with 60 neurons each. Furthermore all networks are trained with an Adam and LFBGS learning rate of $1e - 3$.

5.1 Uniaxial loading

In a first example we study the displacement and stress results from PINN, DEM, mDEM and PINN for a simple uniaxial loading problem as seen in Figure 6a. A $1\text{m} \times 1\text{m}$ block is subjected to a uniform line load on the right-hand

¹Codes will be made public after acceptance of this paper.

side while the movement on the left-hand side is restricted. The FEM solution is generated from a 100×100 elements uniform mesh. The displacement boundary conditions of PINN, DEM and mDEM are a-priori fulfilled by setting

$$\hat{\mathbf{u}}(\mathbf{X}, \boldsymbol{\theta}) = \mathbf{X} \circ \mathbf{z}(\mathbf{X}, \boldsymbol{\theta}). \quad (26)$$

All the methods are trained using a grid of 200×200 training points over the computational domain (see Figure 6b). The boundary traction boundary conditions of PINN and mDEM are trained with an additional 5000 training points per edge. Even though the loading is uniaxial, as the left side of the domain is clamped we are expecting stress concentrations around the top and bottom of that side. After training the networks, the displacement magnitudes of DEM, PINN and

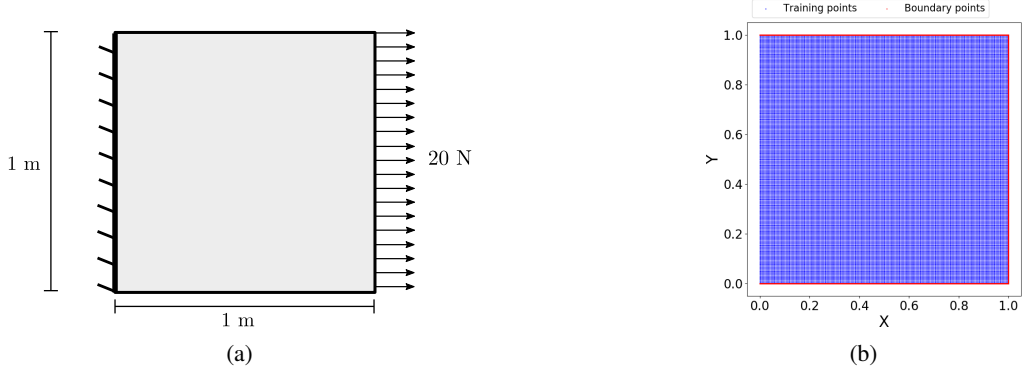


Figure 6: Uniaxial loading problem and training point positions.

mDEM follow the expected pattern providing a relatively good match to the FEM result, as displayed in Figure 7. However the P_{11} and P_{12} stress components approximated by the methods show significant differences, see Figure 8. It is clear that mDEM is able to resolve the stresses that arise near the clamping whereas DEM and PINN fail in doing so.

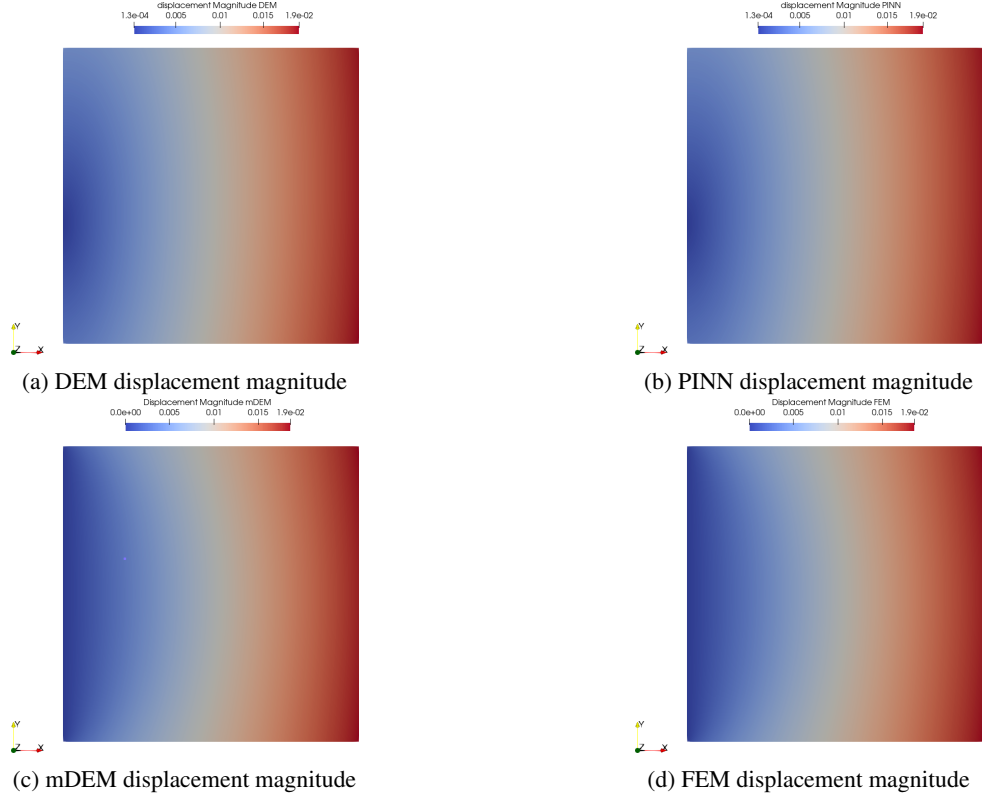


Figure 7: Uniaxial loading problem displacement magnitude.

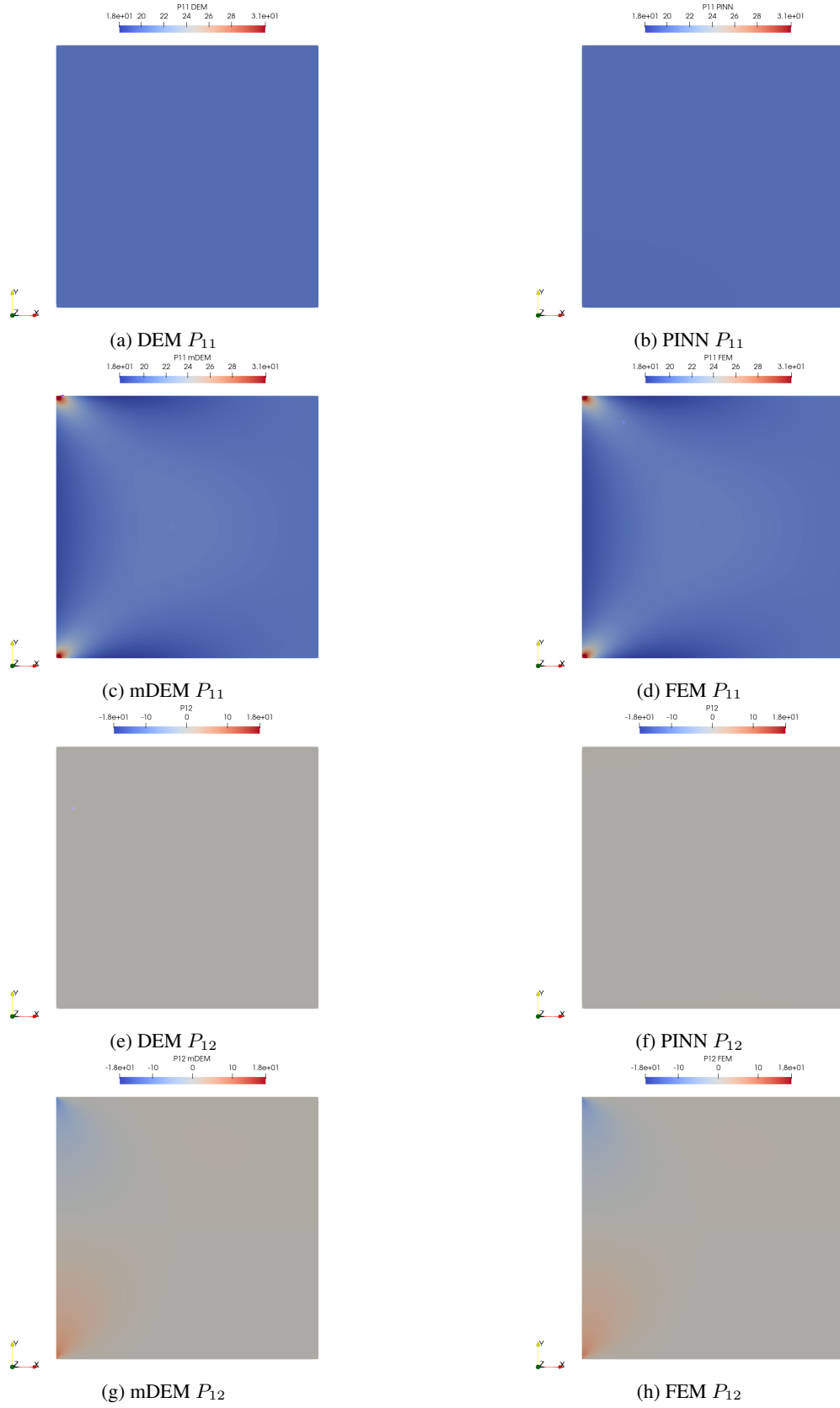


Figure 8: Uniaxial loading problem. P_{11} (a-d) and P_{12} (e-h) stress components.

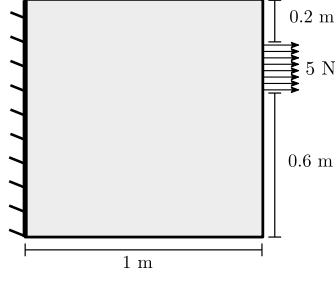


Figure 9: Localized traction problem

5.2 Localized traction boundary

The first example considers the $1m \times 1m$ block as depicted in Figure 9. A load is applied locally on the right-hand side of the block. The same number of domain and boundary training points are used as in the previous example (see Section 5.1 and Figure 6b). The displacement boundary conditions of PINN, DEM and mDEM are a-priori fulfilled by setting

$$\hat{\mathbf{u}}(\mathbf{X}, \boldsymbol{\theta}) = \mathbf{X} \circ \mathbf{z}(\mathbf{X}, \boldsymbol{\theta}). \quad (27)$$

Figure 10 displays the resulting displacement magnitudes of the four different numerical techniques. From the FEM solution it can be seen that there is a displacement concentration around the locally applied traction boundary condition. Comparing DEM, PINN and mDEM results shows that only mDEM is able to resolve this feature accurately. Figure 12a shows the error evolution over the training iterations for PINN. It can be seen that even though the error converges sufficiently, PINN is not able to recover the fine features of the FEM solution, which might be due to the stiffness of problem, i.e. requiring an accurate traction boundary fit on a first order automatic differentiation level while needing to resolve the residual at a second order level. Similarly, the same problems with DEM and PINN can be observed when looking at the resulting stress components P_{11} and P_{12} (Figure 11). In contrast, mDEM is able to achieve proficient stress fields compared to FEM.

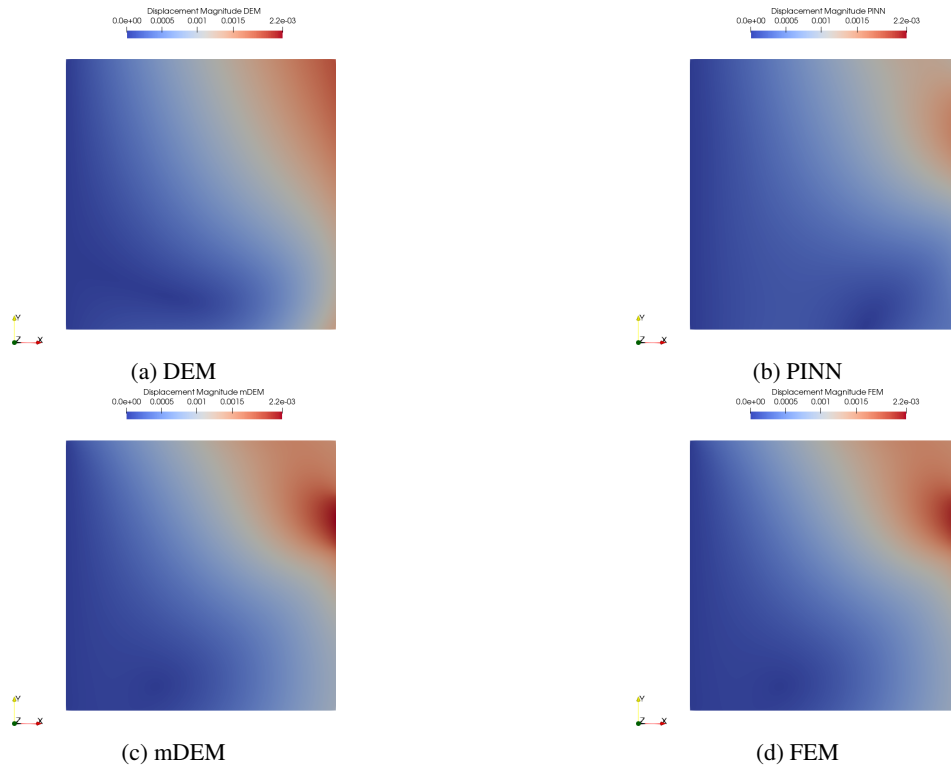


Figure 10: Localized Uniaxial loading problem displacement magnitude.

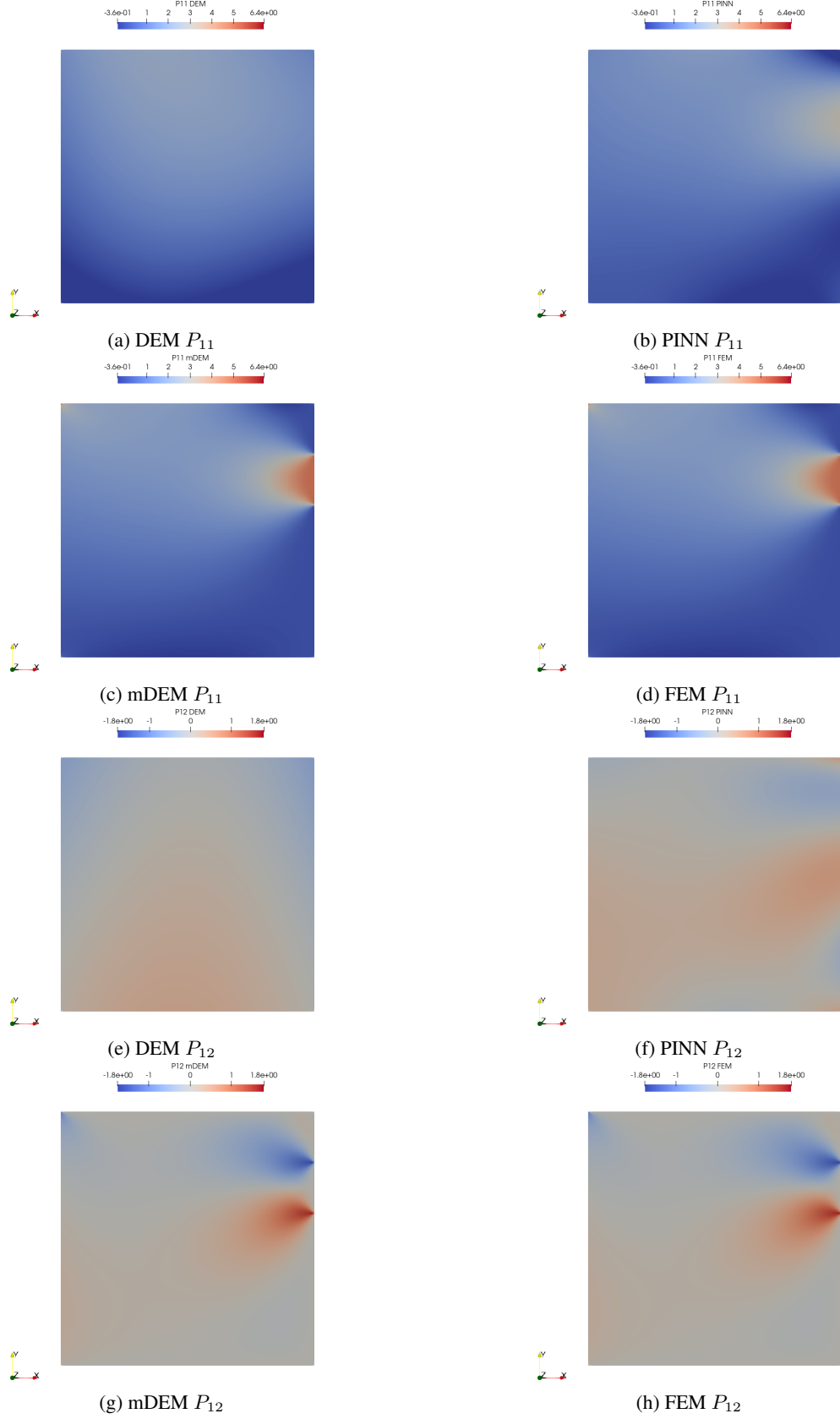


Figure 11: Localized uniaxial loading problem stress components P_{11} (a-d) and P_{12} (e-f).

5.3 Beam with a circular hole

In the last example we look at a 2D beam with a circular hole, see Figure 13a. On each edge 5000 training points for the traction boundary were sampled, whereas the domain training points are arranged in a point-grid of 300×150 samples where points lying in the hole were removed. The final training point positions are displayed in Figure 13b.

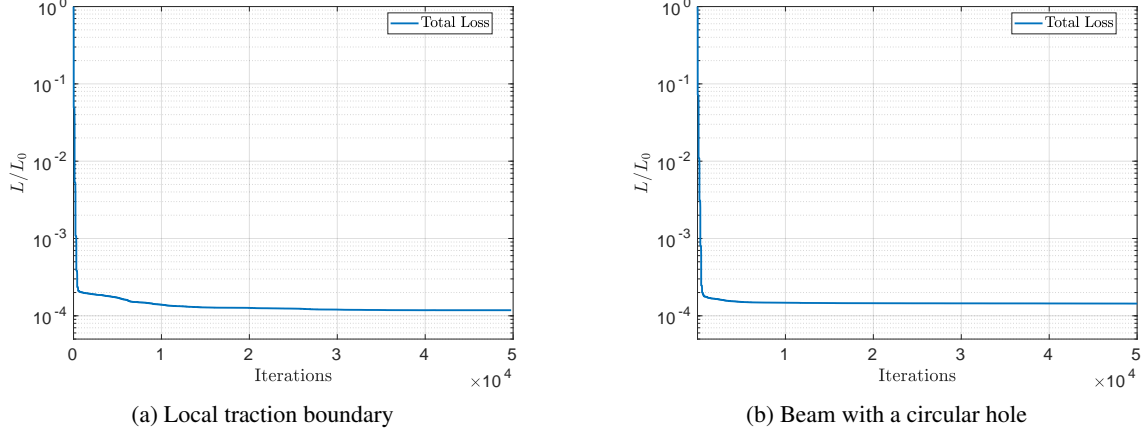


Figure 12: Normalized loss value convergence over iteration steps of PINN.

The displacement boundary conditions of PINN, DEM and mDEM are a-priori fulfilled by defining

$$\begin{aligned} u_1(\mathbf{X}, \boldsymbol{\theta}) &= XY z_1(\mathbf{X}, \boldsymbol{\theta}), \\ u_2(\mathbf{X}, \boldsymbol{\theta}) &= Y z_2(\mathbf{X}, \boldsymbol{\theta}). \end{aligned} \quad (28)$$

The displacement solutions in the x - and y - directions of all investigated techniques are shown in Figure 14 respectively. DEM and mDEM are in close agreement to the FEM solutions, whereas PINN does not appear to find the correct solution. This is supported by the evolution of the loss values over the training procedure as reported in Figure 12b which highlights a quick saturation of the error value pointing towards stagnation in local minima. When looking at the expected stress concentration features, here displayed for the P_{11} and P_{12} components in Figure 15, it can be seen that even though DEM is able to follow the overall stress field in an accurate manner, only mDEM resolves the stress concentrations on comparable levels to FEM.

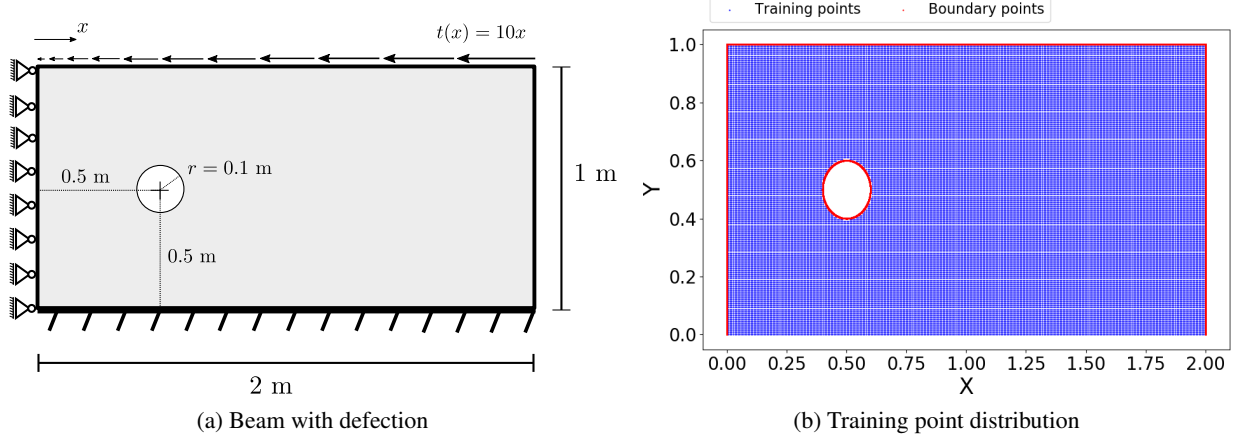


Figure 13: Problem setting and training point positions

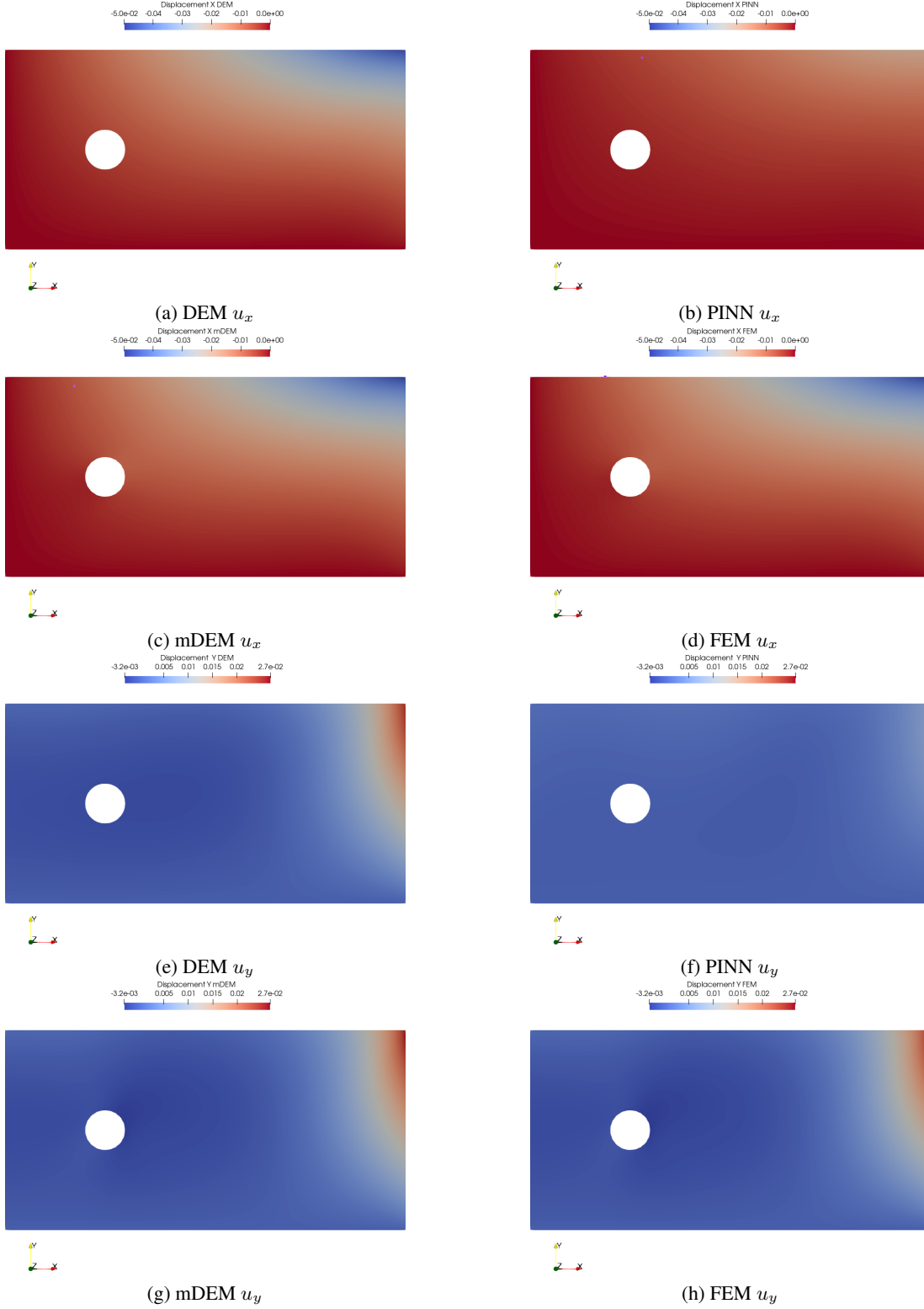


Figure 14: Deflection problem displacement components u_x (a-d) and u_y (e-f) .

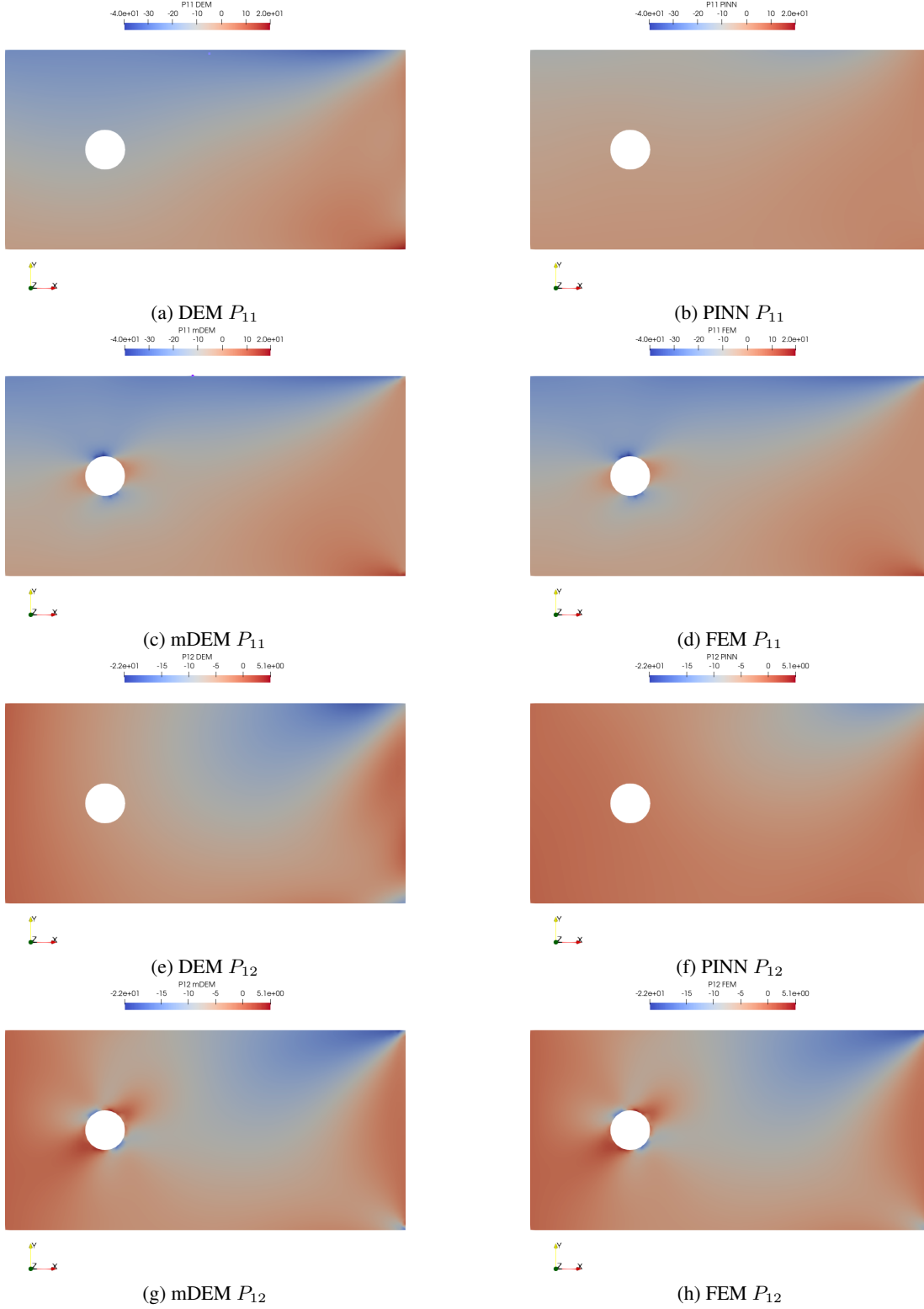


Figure 15: Deflection problem stress components P_{11} (a-d) and P_{12} (e-f).

6 Conclusion and outlook

This paper proposes an extension to the formulation of the Deep Energy Method (DEM) called mixed Deep Energy Method (mDEM). It enhances the original approach which uses a neural network as a global shape function of the displacement over the computational domain by additionally defining the stress components of the first Piola-Kirchhoff stress tensor as outputs of the networks. This proves to be useful in combating the shortcomings of DEM with regards to resolving concentration features. In order to make mDEM more versatile we introduce a numerical integration approach based on Delaunay tessellation that does not require the training point positions to be arranged in grid-like fashion. We test the proposed approach on three computational experiments which exhibit stress concentrations and compare the results to DEM, a Physics-Informed Neural Network and FEM solutions. It can be seen that mDEM is able to yield comparable results to FEM in all investigated problems, whereas DEM and PINN prove to not be reliably able to resolve local stress and displacement features. In future works we plan to apply the presented formulation to three dimensional applications, time-dependent computational experiments as well as problems governed by non-elastic constitutive laws as well as for inverse problems focusing on parameter estimation.

References

- Abueidda, D.W., Lu, Q., Koric, S., 2020. Deep learning collocation method for solid mechanics: Linear elasticity, hyperelasticity, and plasticity as examples. *arXiv preprint arXiv:2012.01547*.
- Alnæs, M.S., Blechta, J., Hake, J., Johansson, A., Kehlet, B., Logg, A., Richardson, C., Ring, J., Rognes, M.E., Wells, G.N., 2015. The fenics project version 1.5. *Archive of Numerical Software* 3. doi:10.11588/ans.2015.100.20553.
- Bottou, L., Curtis, F.E., Nocedal, J., 2018. Optimization methods for large-scale machine learning. *Siam Review* 60, 223–311.
- Eggersmann, R., Kirchdoerfer, T., Reese, S., Stainier, L., Ortiz, M., 2019. Model-free data-driven inelasticity. *Computer Methods in Applied Mechanics and Engineering* 350, 81–99.
- Fuhg, J.N., Boehm, C., Bouklas, N., Fau, A., Wriggers, P., Marino, M., 2021. Model-data-driven constitutive responses: application to a multiscale computational framework. *arXiv:2104.02650*.
- González, D., Chinesta, F., Cueto, E., 2019. Thermodynamically consistent data-driven computational mechanics. *Continuum Mechanics and Thermodynamics* 31, 239–253.
- Goodfellow, I., Bengio, Y., Courville, A., Bengio, Y., 2016. Deep learning. volume 1. MIT press Cambridge.
- Haghighat, E., Raissi, M., Moure, A., Gomez, H., Juanes, R., 2020. A deep learning framework for solution and discovery in solid mechanics. *arXiv preprint arXiv:2003.02751*.
- Hernandez, Q., Badías, A., González, D., Chinesta, F., Cueto, E., 2021. Deep learning of thermodynamics-aware reduced-order models from data. *Computer Methods in Applied Mechanics and Engineering* 379, 113763.
- Hornik, K., Stinchcombe, M., White, H., 1989. Multilayer feedforward networks are universal approximators. *Neural networks* 2, 359–366.
- Huang, D., Fuhg, J.N., Weißenfels, C., Wriggers, P., 2020. A machine learning based plasticity model using proper orthogonal decomposition. *Computer Methods in Applied Mechanics and Engineering* 365, 113008.
- Ibañez, R., Borzacchiello, D., Aguado, J.V., Abisset-Chavanne, E., Cueto, E., Ladeveze, P., Chinesta, F., 2017. Data-driven non-linear elasticity: constitutive manifold construction and problem discretization. *Computational Mechanics* 60, 813–826.
- Jagtap, A.D., Karniadakis, G.E., 2020. Extended physics-informed neural networks (xpinns): A generalized space-time domain decomposition based deep learning framework for nonlinear partial differential equations. *Communications in Computational Physics* 28, 2002–2041.
- Kadeethum, T., Ballarin, F., Bouklas, N., 2021. Non-intrusive reduced order modeling of poroelasticity of heterogeneous media based on a discontinuous galerkin approximation. *arXiv preprint arXiv:2101.11810*.
- Kadeethum, T., Jørgensen, T.M., Nick, H.M., 2020. Physics-informed neural networks for solving nonlinear diffusivity and biot’s equations. *PloS one* 15, e0232683.
- Kharazmi, E., Zhang, Z., Karniadakis, G.E., 2021. hp-vpinns: Variational physics-informed neural networks with domain decomposition. *Computer Methods in Applied Mechanics and Engineering* 374, 113547.
- Kingma, D.P., Ba, J., 2014. Adam: A method for stochastic optimization. *arXiv preprint arXiv:1412.6980*.
- Kirchdoerfer, T., Ortiz, M., 2016. Data-driven computational mechanics. *Computer Methods in Applied Mechanics and Engineering* 304, 81–101.
- Lagaris, I.E., Likas, A., Fotiadis, D.I., 1998. Artificial neural networks for solving ordinary and partial differential equations. *IEEE transactions on neural networks* 9, 987–1000.
- Nguyen-Thanh, V.M., Zhuang, X., Rabczuk, T., 2020. A deep energy method for finite deformation hyperelasticity. *European Journal of Mechanics-A/Solids* 80, 103874.
- Paszke, A., Gross, S., Massa, F., Lerer, A., Bradbury, J., Chanan, G., Killeen, T., Lin, Z., Gimelshein, N., Antiga, L., Desmaison, A., Kopf, A., Yang, E., DeVito, Z., Raison, M., Tejani, A., Chilamkurthy, S., Steiner, B., Fang, L., Bai, J., Chintala, S., 2019. Pytorch: An imperative style, high-performance deep learning library, in: Wallach, H., Larochelle, H., Beygelzimer, A., d’Alché-Buc, F., Fox, E., Garnett, R. (Eds.), *Advances in Neural Information Processing Systems* 32. Curran Associates, Inc., pp. 8024–8035. URL: <http://papers.neurips.cc/paper/9015-pytorch-an-imperative-style-high-performance-deep-learning-library.pdf>.
- Raissi, M., Perdikaris, P., Karniadakis, G.E., 2019. Physics-informed neural networks: A deep learning framework for solving forward and inverse problems involving nonlinear partial differential equations. *Journal of Computational Physics* 378, 686–707.

- Rao, C., Sun, H., Liu, Y., 2020. Physics informed deep learning for computational elastodynamics without labeled data. arXiv preprint arXiv:2006.08472 .
- Samaniego, E., Anitescu, C., Goswami, S., Nguyen-Thanh, V.M., Guo, H., Hamdia, K., Zhuang, X., Rabczuk, T., 2020. An energy approach to the solution of partial differential equations in computational mechanics via machine learning: Concepts, implementation and applications. *Computer Methods in Applied Mechanics and Engineering* 362, 112790.
- Weinan, E., Yu, B., 2018. The deep ritz method: a deep learning-based numerical algorithm for solving variational problems. *Communications in Mathematics and Statistics* 6, 1–12.